PHYSICS

Prediction of giant and ideal Rashba-type splitting in ordered alloy monolayers grown on a polar surface

Mingxing Chen [ID][1,*] and Feng Liu[2]

ABSTRACT

A large and ideal Rashba-type spin-orbit splitting is desired for the applications of materials in spintronic devices and the detection of Majorana fermions in solids. Here, we propose an approach to achieve giant and ideal spin-orbit splittings through a combination of ordered surface alloying and interface engineering, that is, growing alloy monolayers on an insulating polar surface. We illustrate this unique strategy by means of first-principle calculations of buckled hexagonal monolayers of SbBi and PbBi supported on $Al_2O_3(0001)$. Both systems display ideal Rashba-type states with giant spin-orbit splittings, characterized with energy offsets over 600 meV and momentum offsets over 0.3 Å^{-1}, respectively. Our study thus points to an effective way of tuning spin-orbit splitting in low-dimensional materials to draw immediate experimental interest.

Keywords: Rashba effect, interface, spin-orbit coupling

[1]Key Laboratory for Matter Microstructure and Function of Hunan Province, Key Laboratory of Low-Dimensional Quantum Structures and Quantum Control of Ministry of Education, Synergetic Innovation Center for Quantum Effects and Applications (SICQEA), School of Physics and Electronics, Hunan Normal University, Changsha 410081, China and [2]Department of Materials Science and Engineering, University of Utah, Salt Lake City, UT 84112, USA

*Corresponding author. E-mail: mxchen@hunnu.edu.cn

INTRODUCTION

The Rashba effect is referred to as the spin-orbit (SO) splitting at surfaces/interfaces due to the broken inversion symmetry [1,2], which has led to many exotic quantum phenomena and novel applications, ranging from the spin Hall effect, Majorana fermions in solids and the spin field-effect transistor [3–5]. The effective Rashba Hamiltonian for an electron with momentum **k** and spin σ can be written as

$$\hat{H}_R = \lambda \sigma \cdot (\mathbf{E_z} \times \mathbf{k}),$$

where λ is the strength of the SO coupling (SOC) and $\mathbf{E_z}$ is the electric field perpendicular to the surface/interface created by a perpendicular potential gradient related to the structural asymmetry. The SO splitting is defined as $\alpha_R = 2E_R/k_R$, where E_R and k_R are the Rashba energy and momentum offset, respectively.

In the ongoing exploration of large Rashba-type SO splittings in materials, enhancing the strength of λ by introducing heavy elements has been extensively used [6–11]. In particular, the ordered $(\sqrt{3} \times \sqrt{3})$ superstructure of Bi/Ag(111) in which one surface Ag is replaced by Bi displays a giant Rashba energy offset (E_R) of 200 meV and momentum offset (k_R) of 0.13 Å^{-1} [6]. In addition,

semiconducting substrates are used to avoid the mixing of the Rashba states and the spin-degenerate substrate states, in order to create so-called ideal Rashba states [12–22]. On the other hand, the interfacial dipole field can be used to enhance $\mathbf{E_z}$ and hence the SO splitting. Polar semiconductors are effective substrates to serve this purpose [22–27]. In fact, the surfaces of polar semiconductors bismuth tellurohalides BiTeX (X = Cl, Br and I) have been found to exhibit giant SO splittings [28,29]. Moreover, the Rashba SO splitting can be controlled by the electric polarization in ferroelectric materials and substrates [23–25,30–32]. Despite these achievements, natural materials exhibiting both giant and ideal Rashba states are rare. Therefore, artificial interfaces by *a priori* theoretical design are highly desirable to fill this outstanding gap.

In this work, we demonstrate the design principle to create giant and ideal interfacial Rashba states by combining ordered surface alloying and growth on a polar insulator/semiconductor surface. Using density-functional theory (DFT) calculations, we show unprecedented large Rashba energy offsets over 600 meV and momentum offsets over 0.3 Å^{-1} for both SbBi/Al$_2$O$_3$(0001) and PbBi/Al$_2$O$_3$(0001), which are roughly three times of those in Bi/Ag(111). Also, such Rashba

states are ideally situated inside the band gap of $Al_2O_3(0001)$.

RESULTS

We begin by illustrating the general idea as shown in Fig. 1. Our structural model makes use of the geometric and electronic properties of both the buckled overlayer and substrate. The buckled honeycomb structure exists in a number of elemental layered materials, such as silicene, germanene, stanene and Bi(111) monolayers [33–37], which consist of two trigonal sublattices sitting at different heights. Now imagine that these two sublattices are made of different types of atoms to break inversion symmetry. Then a Rashba SO splitting will arise in such a buckled honeycomb alloy monolayer. Apparently, to enhance SOC, the optimal choice to form the monolayer are heavy atoms, such as Bi, Pb and Sb. This constitutes our first idea of the surface alloying effect. Next, let us imagine growing this alloy monolayer on a polar insulator/semiconductor substrate. The polar surface induces an additional perpendicular potential gradient (ΔV_i) through the alloy monolayer. If ΔV_i is along the same direction as the alloying induced potential gradient ΔV_a, then it will further enhance ΔV_a (see Fig. 1(d)). Consequently, the combined effects of surface alloying and the polar surface conspire, leading to a giant SO in the monolayer. By properly choosing the monolayer-substrate material combinations, we

can further tune the relative positions of monolayer SO states relative to that of the substrate band gap to achieve ideal Rashba-type states.

To validate our idea we performed DFT calculations for buckled monolayers of Bi (Bi-1L), Pb (Pb-1L), Sb and their ordered alloys on $Al_2O_3(0001)$. $Al_2O_3(0001)$ is chosen for several reasons. First, it has been extensively used as a substrate for the growth of various materials. Second, there are two different types of atoms in the surface, i.e. Al and O, which behave chemically different. In addition, the surface Al atom is slightly higher (~0.15 Å) than the O atom, which is beneficial for growing the buckled monolayers. Therefore, we may expect an enhanced SO splitting when two different atoms in the overlayer bind to Al and O. Moreover, it has a large band gap, which is favorable for forming ideal Rashba states.

We have systematically evaluated the structures and energetics of our systems. The low-energy structures were derived from our previous calculations of stanene/$Al_2O_3(0001)$ using the CALYPSO structure prediction method [38], which produced the same structure for stanene/$Al_2O_3(0001)$ as reported in [39]. For the homonuclear monolayers, the structure is shown in Fig. 2. The overlayers preserve the buckled honeycomb structure upon geometric relaxation and have a strong binding with the substrate. The structural properties and energetics are given in Fig. S1.

We first discuss the interfacing effect on the SO splitting in homonuclear monolayers, i.e. Bi/$Al_2O_3(0001)$ and Pb/$Al_2O_3(0001)$. In Fig. 2 we show the band structures for Bi/$Al_2O_3(0001)$ and Pb/$Al_2O_3(0001)$ with and without SOC, respectively, which reveals that both are semiconductors with a gap of about 0.30 eV when SOC is included. The most prominent feature is the large SO splittings in the overlayer due to the presence of a substrate compared to those of the free-standing monolayers [36,37,40]. For Bi/$Al_2O_3(0001)$, the conduction band shows a Rashba-like splitting. While for Pb/$Al_2O_3(0001)$, the Rashba-like splitting appears in the valance band. For Pb/$Al_2O_3(0001)$, there are two series of Rashba-type bands mixed near Γ. They become distinct by increasing the layer distance (Fig. S2). Orbital projections reveal that the bands near the gap are basically contributed by the *p* orbitals of Bi (Pb) (Fig. S3). Thus, the Rashba states are ideal in Bi/$Al_2O_3(0001)$ and Pb/$Al_2O_3(0001)$.

We have checked the spin texture of the Rashba states by plotting spin projections onto the direction vector of $\mathbf{K} \times \mathbf{e}_z$ for the bands of the two systems, where $\mathbf{K} = (1/3, 1/3, 0)$ and $\mathbf{e}_z = (0, 0, 1)$ is the unit vector normal to the surface. The in-plane component perpendicular (parallel/antiparallel) to
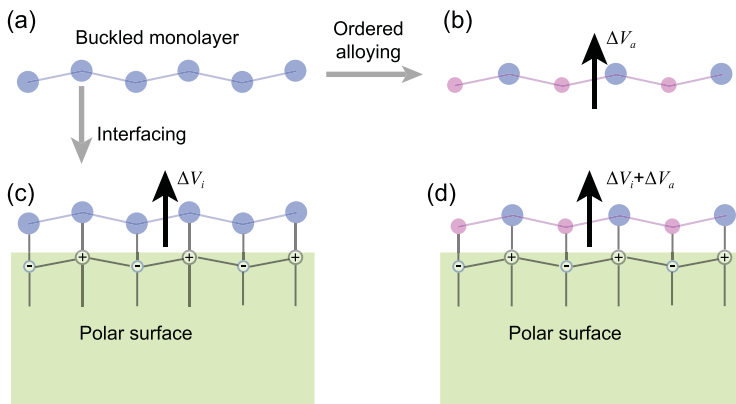

Figure 1. Sketch of manipulating the potential gradient through a buckled monolayer by ordered alloying and interfacing. (a) The geometry of a free-standing buckled monolayer. (b) Perpendicular potential gradient (ΔV_a) induced by ordered alloying. (c) Interface-induced potential gradient (ΔV_i) through the monolayer when placing it onto a polar surface, e.g. growing it on a substrate. A large ΔV_i can be favored when they form a special interface structure such that the two atoms in the monolayer bind to different types of ions in a polar surface. (d) The combined effect of the ordered alloying and interfacing. The arrows indicate the perpendicular potential gradients. Different types of atoms are in different colors. The $+/-$ symbols represent cations/anions in the polar surface.
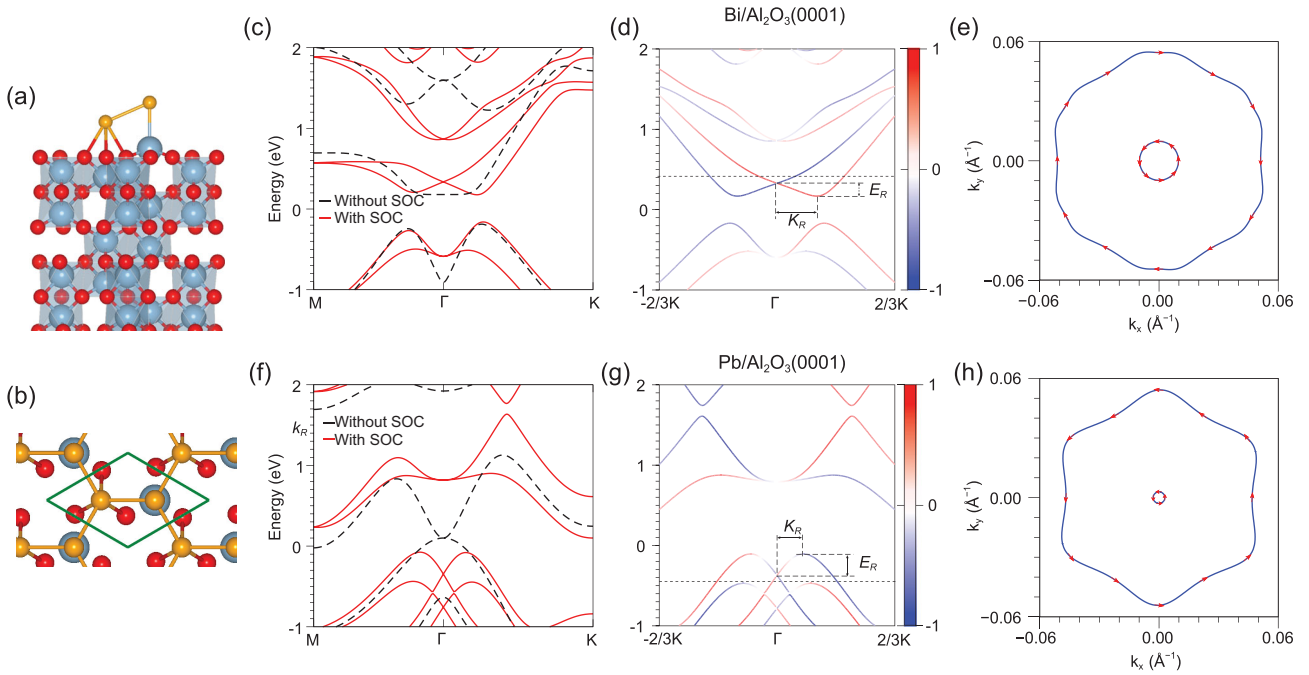
Figure 2. SO splittings in Bi/Al$_2$O$_3$(0001) and Pb/Al$_2$O$_3$(0001). (a, b) Side and top views of the monolayer supported on Al$_2$O$_3$(0001). The Al and O atoms are denoted by silver and red balls, respectively. The green box in (b) represents the primitive cell of the interface structure. (c, f) The band structures of Bi/Al$_2$O$_3$(0001) and Pb/Al$_2$O$_3$(0001), respectively. The red solid lines denote the bands derived from SOC calculations, whereas the black dashed lines represent the bands from nonrelativistic calculations. (d) Spin projections onto the direction vector of $\mathbf{K} \times \mathbf{e}_z$ for bands along $-$K-$\Gamma$$-$K, where $\mathbf{e}_z = (0, 0, 1)$, for Bi/Al$_2$O$_3$(0001). Blue and red represent positive and negative spin polarizations, respectively. (e) The Fermi surfaces for the energy marked in (b) by the dashed line. (g, h) Corresponding plots for Pb/Al$_2$O$_3$(0001). The red arrows in (e) and (h) denote the spin polarizations. We mark E_R and k_R for the bands discussed in the text. The Fermi level is set to zero.

the vector is denoted by $S_\perp$ ($S_\parallel$), while the out-of-plane component is denoted by S_z. In Fig. 2(b) and (e) we show the bands weighted by $S_\parallel$ along $-$K-$\Gamma$$-$K, and in Fig. 2(c) and (f) we show the Fermi surface and spin texture for the energy marked in (b) and (c), respectively. For the conduction band of Bi/Al$_2$O$_3$(0001), S_z and $S_\perp$ are negligible, confirming the Rashba nature of this band, although the outer branch undergoes a slight warping compared with the inner branch. For the valance band of Pb/Al$_2$O$_3$(0001), the warping becomes more prominent and S_z is relatively more appreciable than that for Bi/Al$_2$O$_3$(0001). The warping indicates that the SO splitting is anisotropic, which has the largest value along Γ–K. We marked the Rashba energy offset E_R and momentum offset k_R in Fig. 2(b) and (e). For Bi/Al$_2$O$_3$(0001), E_R is about 160 meV, comparable to that for Bi/Ag(111) (200 meV). Such an SO splitting is one order of magnitude larger than that for the pure Bi(111) (10 meV) [41]. While k_R is about 0.2 Å^{-1}, which is 50% larger than that for Bi/Ag(111). For Pb/Al$_2$O$_3$(0001), E_R is about 260 meV, which is about 30% larger than that for Bi/Ag(111). The enhancement in E_R leads to a larger α_R for Pb/Al$_2$O$_3$(0001) compared

to Bi/Ag(111), since k_R is basically the same for both.

The large SO splitting can be further enhanced by appropriate ordered alloying. We substitute one Bi in Bi-1L by an Sb atom, which allows us to obtain a semiconducting monolayer, while replacing one Bi by Pb leads to split states crossing the Fermi level. The band structures for the lowest-energy structure for SbBi/Al$_2$O$_3$(0001) and PbBi/Al$_2$O$_3$(0001) are shown in Fig. 3. Note that the splitting is now strongly anisotropic compared to that for homonuclear monolayers. For SbBi/Al$_2$O$_3$(0001), the bands are pretty much similar to those for Bi/Al$_2$O$_3$(0001). However, E_R is increased to about 640 meV and k_R is about 0.36 Å^{-1} for the conduction band along Γ–K. Likewise, we obtain a giant SO splitting for PbBi/Al$_2$O$_3$(0001), for which the energy offset is as large as 740 meV and k_R is about 0.34 Å^{-1} for the bands crossing the Fermi level.

The large SO splitting is further confirmed by hybrid density-functional calculations (see Fig. S4). We further demonstrate that the large SO splittings are maintained even when the chemical composition is not ideal. To show this effect, we have performed calculations for Sb$_{1.1}$Bi$_{0.9}$/Al$_2$O$_3$(0001)
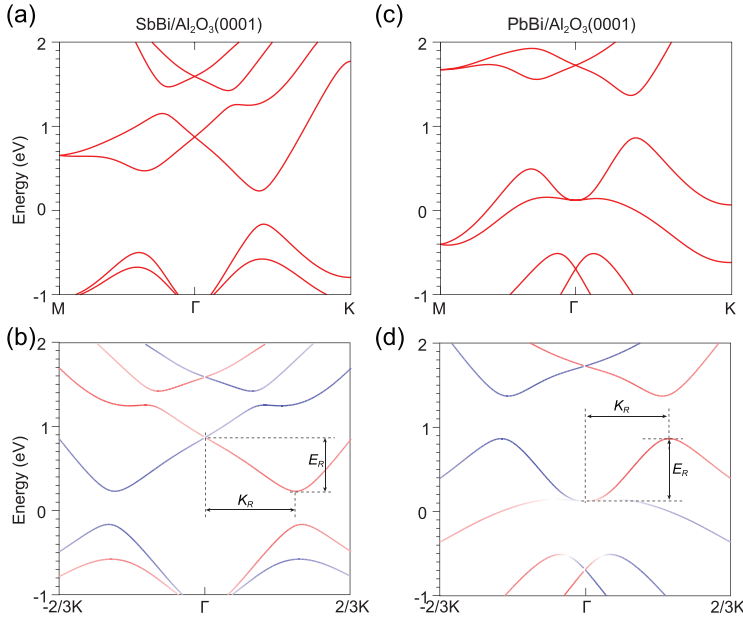
(a)

SbBi/Al$_2$O$_3$(0001)

(c)

PbBi/Al$_2$O$_3$(0001)

(b)

(d)

Figure 3. SO splittings in ordered alloy monolayers on Al$_2$O$_3$(0001). (a, c) Band structures of SbBi/Al$_2$O$_3$(0001) and PbBi/Al$_2$O$_3$(0001), respectively. (b, d) Corresponding spin projections onto the direction vector of $\mathbf{K} \times \mathbf{e}_z$ for bands along $-$K-Γ-K. The Fermi level is set to zero.

and Sb$_{0.9}$Bi$_{1.1}$/Al$_2$O$_3$(0001) using the virtual crystal approximation to mimic a random alloy. Our calculations reveal that a 10% deviation from the ideal chemical composition has only a minor effect on the SO splitting (see Fig. S5). Moreover, to see the effect of the buckling height on the SO splitting, we carried out two additional calculations for SbBi/Al$_2$O$_3$(0001) with two different buckling heights. The structures were obtained by artificially adjusting the z value of Sb by ± 0.1 Å, which gives about an 8% change in the buckling height. As a result, E_R and k_R change by about 10% (see Fig. S6). However, we may expect that the buckling height in an experimentally grown sample should be rather close to the optimized value by our calculations.

In Table 1, we summarize the Rashba parameter α_R, energy offset E_R and momentum offset k_R for the systems studied. Here E_R and k_R are for the bands marked in Figs 2 and 3. We also show the SO splitting parameters of the heavy-element doped nonpolar surface Bi/Ag(111) and the surface of polar semiconductor BiTeI for comparison. For the alloy systems SbBi/Al$_2$O$_3$(0001) and PbBi/Al$_2$O$_3$(0001), E_R is over 640 meV along $-$K-Γ-K, which is more than three times that of Bi/Ag(111) and six times that of the surface of BiTeI. While k_R is almost three times that of Bi/Ag(111) and one order of magnitude larger than BiTeI. Consequently, an unprecedentedly large Rashba parameter α_R is obtained for both SbBi/Al$_2$O$_3$(0001) and PbBi/Al$_2$O$_3$(0001). Compared to the isolated system, e.g. SbBi, inter-

facing with Al$_2$O$_3$(0001) enhances E_R by a factor of three and enhances α_R by a factor of roughly two. Our results thus demonstrate that the combination of ordered alloying and interfacing with a polar surface can be an effective strategy to obtain a giant SO splitting in buckled monolayers.

The large SO splittings originate from the special geometry that induces a large perpendicular potential gradient through the overlayer. Within the tight-binding approximation, the effect of the perpendicular potential gradient goes into on-site Hamiltonian matrix elements. We perform analyses on the Hamiltonian matrix elements as derived from the linear combination of the atomic orbital calculation [42], which reproduced the band structures shown in Figs 2 and 3 (see Fig. S7). In Table 2 we list the differences in the on-site Hamiltonian matrix elements for the p orbital between the two atoms in the overlayer, denoted as $\Delta H_{\alpha,\alpha}$, for which the atom binding to the oxygen atom is taken as the reference. For the freestanding Bi-1L and Pb-1L, the $\Delta H_{\alpha,\alpha}$ are zeros, which become greater than 0.5 eV when supported on Al$_2$O$_3$(0001). The interface-induced perpendicular electric field through the supported Bi-1L is about 0.5 eV/Å, estimated by $\Delta H_{p_z,p_z}/\Delta z$. The estimated E_z for Pb-1L is double that of Bi-1L. This trend is consistent with the fact that α_R for Pb/Al$_2$O$_3$(0001) is much larger than that for Bi/Al$_2$O$_3$(0001) (see Table 1). The difference between $\Delta H_{p_x,p_x}$ ($\Delta H_{p_y,p_y}$) and $\Delta H_{p_z,p_z}$ is attributed to the two-dimensional nature of the interface structure.

For the ordered alloy systems SbBi and PbBi, the structure naturally gives a difference in the on-site Hamiltonian matrix elements, which results in SO splittings in the electronic bands (Fig. S8). From Table 2 we can see that the $\Delta H_{\alpha,\alpha}$ are enhanced by over 0.6 eV for the supported SbBi. For PbBi, interfacing reverses the potential gradient, which leads to changes in $\Delta H_{\alpha,\alpha}$ over 0.8 eV for the p orbital. Consequently, the SO splitting is significantly enhanced by interfacing compared to that for the isolated monolayer alloy.

In addition to the giant SO splittings, some of our systems may have nontrivial topological properties. We have calculated the evolution of the Wannier function center based on the method proposed in [43]. Our results reveal that Pb/Al$_2$O$_3$(0001) and Bi/Al$_2$O$_3$(0001) have a Z_2 equal to one (Fig. S9), whereas SbBi/Al$_2$O$_3$(0001) has a Z_2 equal to zero (not shown). We further performed calculations of edge states by making the surface monolayer into a nanoribbon. Our calculations show that there are gapless edge states for Pb/Al$_2$O$_3$(0001) and Bi/Al$_2$O$_3$(0001) (Fig. S9). Thus, these two systems are expected to be topologically nontrivial.

Table 1. SO splitting in buckled monolayers on $Al_2O_3(0001)$ and selected materials from the literature. Here E_R and k_R are the Rashba energy offset and momentum offset for the bands marked in Figs 2 and 3, and α_R is the Rashba parameter calculated by $\alpha_R = 2E_R/k_R$. The identity indicates whether the Rashba-type states mix with the substrate states.

Materials	E_R (meV)	k_R (Å^{-1})	α_R (eVÅ)	Identity	Reference
Heavy-element doped nonpolar surface					
Bi/Ag(111)	200	0.13	3.05	Mixed	[6]
Polar surface					
BiTeI	108	0.05	4.30	Ideal	[29]
Homolayer on polar surface					
Au/InSe(0001)	–	–	0.45	Ideal	[22]
Bi/Al$_2$O$_3$(0001)	160	0.20	1.61	Ideal	This work
Pb/Al$_2$O$_3$(0001)	266	0.13	4.14	Ideal	This work
Isolated ordered alloy monolayer					
SbBi	150	0.21	1.40	Ideal	This work
Ordered alloy monolayer on polar surface					
SbBi/Al$_2$O$_3$(0001)	641	0.36	3.55	Ideal	This work
PbBi/Al$_2$O$_3$(0001)	741	0.34	4.38	Ideal	This work

Table 2. Effects of alloying and interfacing on the on-site hopping parameters ($H_{\alpha,\alpha}$) for the monolayers on Al$_2$O$_3$(0001). Here $\Delta H_{\alpha,\alpha}$ is the difference in the on-site hopping terms for orbital α between the two atoms in the over-layer, which takes the atom binding to the oxygen atoms as the reference, and Δz denotes the buckling in the overlayer.

Materials	$\Delta H_{p_x,p_x}$ (eV)	$\Delta H_{p_y,p_y}$ (eV)	$\Delta H_{p_z,p_z}$ (eV)	Δz (Å)
Pb/Al$_2$O$_3$(0001)	0.83	0.83	1.32	1.30
Bi/Al$_2$O$_3$(0001)	0.58	0.58	0.73	1.50
Isolated SbBi	0.20	0.20	0.68	1.25
SbBi/Al$_2$O$_3$(0001)	1.07	1.07	1.31	1.25
Isolated PbBi	−0.46	−0.46	−0.68	1.37
PbBi/Al$_2$O$_3$(0001)	0.37	0.37	0.64	1.37

Lastly, we discuss the experimental feasibility of our systems. The layered crystal structure of bismuth favors the growth of Bi-1L, which has been obtained on several semiconducting substrates such as Bi$_2$Te$_3$ and Bi$_2$Se$_3$ by molecular beam epitaxy (MBE) growth [44–46]. While the buckled honeycomb structure of Pb was predicted to be energetically lower than the planar one [40]. Alloy systems such as Sb$_{1−x}$Bi$_x$ and Pb$_{1−x}$Bi$_x$ have been grown on Ag(111) [8–10]. Moreover, Pb-based and Bi-based ordered alloys on surfaces, e.g. Tl$_3$Pb/Si(111) and Sn$_2$Bi/Si(111), have also been obtained in recent experiments [18,21]. Regarding the substrate, Al$_2$O$_3$(0001) has been extensively used as a substrate for the growth of thin films. For instance, it has been used for the growth of silicene [47], confirming our early DFT prediction [48]. Our calculations show that the binding energy (E_b) is about 0.25 eV/Bi for Bi/Al$_2$O$_3$(0001), much larger

than that for Bi/Bi$_2$Te$_3$ (0.10 eV/Bi), a system already obtained in the laboratory [44]. While for Pb/Al$_2$O$_3$(0001) and the alloy systems, E_b is larger than 0.50 eV/atom, favoring the monolayer structure. For isolated SbBi, a previous study found that it is both dynamically and thermodynamically stable [20]. We further performed an *ab initio* molecular dynamics simulation ($T = 500$ K) for the supported system, i.e. SbBi/Al$_2$O$_3$(0001), which shows that the structure is also thermodynamically stable (Fig. S10). Therefore, the growth of our systems can be highly feasible.

CONCLUSION

In summary, we have proposed a strategy that combines the surface alloying and interface engineering to manipulate the SO splitting in two-dimensional materials. We have illustrated the idea in low-buckled hexagonal monolayers, e.g. Bi-1L, Pb-1L and their alloys SbBi and PbBi, supported on Al$_2$O$_3$(0001) by DFT calculations. Our calculations show giant Rashba-like SO splittings in these interface structures. In particular, the Rashba energies and momentum offsets of the split states for SbBi/Al$_2$O$_3$(0001) and PbBi/Al$_2$O$_3$(0001) are roughly three times those of Bi/Ag(111). Our study thus provides an effective way of manipulating the SO splitting in layered two-dimensional materials for potential applications in spintronics and the study of Majorana fermions in solids.

METHODS

Our calculations were performed using the Vienna Ab Initio Simulation Package [49]. The interface

structure was modeled in terms of a repeated slab, separated from its periodic images by 10 Å vacuum regions. We note that the lattice mismatch strain can be effectively relieved by adjusting the buckling height of the overlayer [45,46]. Therefore, the interface structure in our modeling contains only one unit cell for both the overlayer and the substrate. The pseudopotentials were constructed by the projector augmented wave method [50]. Van der Waals (vdW) dispersion forces between the adsorbate and the substrate were accounted for through the optimized Perdew–Burke–Ernzerhof density functional by using the vdW density-functional method [51]. A 11×11 Γ-centered Monkhorst-Pack k-point mesh was used to sample the surface Brillouin zone. A plane-wave energy cutoff of 400 eV was used for all the calculations. The overlayer atoms and the surface Al and O atoms were fully relaxed until the residual forces were less than 0.001 eV/Å.

SUPPLEMENTARY DATA

Supplementary data are available at *NSR* online.

FUNDING

AUTHOR CONTRIBUTIONS

M.C. proposed the project and carried out the calculations. Both authors contributed to the analysis of the data and the manuscript writing.

Conflict of interest statement. None declared.

REFERENCES

1. Bychkov YA and Rashba ÉI. Properties of a 2D electron gas with lifted spectral degeneracy. *JETP Lett* 1984; **39**: 78–81.
2. Caviglia AD, Gabay M and Gariglio S *et al.* Tunable Rashba spin-orbit interaction at oxide interfaces. *Phys Rev Lett* 2010; **104**: 126803.
3. Sinova J, Culcer D and Niu Q *et al.* Universal intrinsic spin Hall effect. *Phys Rev Lett* 2004; **92**: 126603.
4. Qi XL and Zhang SC. Topological insulators and superconductors. *Rev Mod Phys* 2011; **83**: 1057–110.
5. Datta S and Das B. Electronic analog of the electro-optic modulator. *Appl Phys Lett* 1990; **56**: 665–7.
6. Ast CR, Henk J and Ernst A *et al.* Giant spin splitting through surface alloying. *Phys Rev Lett* 2007; **98**: 186807.
7. Bihlmayer G, Blügel S and Chulkov EV. Enhanced Rashba spin-orbit splitting in Bi/Ag(111) and Pb/Ag(111) surface alloys from first principles. *Phys Rev B* 2007; **75**: 195414.
8. Ast CR, Pacilé D and Moreschini L *et al.* Spin-orbit split two-dimensional electron gas with tunable Rashba and Fermi energy. *Phys Rev B* 2008; **77**: 081407.
9. Meier F, Petrov V and Guerrero S *et al.* Unconventional Fermi surface spin textures in the Bi$_x$Pb$_{1-x}$/Ag(111) surface alloy. *Phys Rev B* 2009; **79**: 241408.
10. Gierz I, Meier F and Dil JH *et al.* Tuning the spin texture in binary and ternary surface alloys on Ag(111). *Phys Rev B* 2011; **83**: 195122.
11. Moreschini L, Bendounan A and Bentmann H *et al.* Influence of the substrate on the spin-orbit splitting in surface alloys on (111) noble-metal surfaces. *Phys Rev B* 2009; **80**: 035438.
12. Sakamoto K, Oda T and Kimura A *et al.* Abrupt rotation of the Rashba spin to the direction perpendicular to the surface. *Phys Rev Lett* 2009; **102**: 096805.
13. Frantzeskakis E, Pons S and Grioni M. Band structure scenario for the giant spin-orbit splitting observed at the Bi/Si(111) interface. *Phys Rev B* 2010; **82**: 085440.
14. Stolwijk SD, Sakamoto K and Schmidt AB *et al.* Thin line of a Rashba-type spin texture: unoccupied surface resonance of Tl/Si(111) along $\overline{\Gamma M}$. *Phys Rev B* 2014; **90**: 161109.
15. Hatta S, Aruga T and Kato C *et al.* Band structure of Tl/Ge(111)-(3 × 1): angle-resolved photoemission and first-principles prediction of giant Rashba effect. *Phys Rev B* 2008; **77**: 245436.
16. Yaji K, Ohtsubo Y and Hatta S *et al.* Large Rashba spin splitting of a metallic surface-state band on a semiconductor surface. *Nat Commun* 2010; **1**: 17.
17. Gruznev DV, Bondarenko LV and Matetskiy AV *et al.* A strategy to create spin-split metallic bands on silicon using a dense alloy layer. *Sci Rep* 2014; **4**: 4742.
18. Matetskiy AV, Ichinokura S and Bondarenko LV *et al.* Two-dimensional superconductor with a giant Rashba effect: one-atom-layer Tl-Pb compound on Si(111). *Phys Rev Lett* 2015; **115**: 147003.
19. Gruznev DV, Bondarenko LV and Matetskiy AV *et al.* Synthesis of two-dimensional Tl$_x$Bi$_{1-x}$ compounds and Archimedean encoding of their atomic structure. *Sci Rep* 2016; **6**: 19446.
20. Singh S and Romero AH. Giant tunable Rashba spin splitting in a two-dimensional BiSb monolayer and in BiSb/AlN heterostructures. *Phys Rev B* 2017; **95**: 165444.
21. Gou J, Xia B and Li H *et al.* Binary two-dimensional honeycomb lattice with strong spin-orbit coupling and electron-hole asymmetry. *Phys Rev Lett* 2018; **121**: 126801.
22. Ming W, Wang ZF and Zhou M *et al.* Formation of ideal Rashba states on layered semiconductor surfaces steered by strain engineering. *Nano Lett* 2016; **16**: 404–9.
23. Mirhosseini H, Maznichenko IV and Abdelouahed S *et al.* Toward a ferroelectric control of Rashba spin-orbit coupling: Bi on BaTiO$_3$(001) from first principles. *Phys Rev B* 2010; **81**: 073406.
24. Lutz P, Figgemeier T and El-Fattah ZMA *et al.* Large spin splitting and interfacial states in a Bi/BaTiO$_3$(001) Rashba ferroelectric heterostructure. *Phys Rev Appl* 2017; **7**: 044011.

25. Zhong Z, Si L and Zhang Q *et al.* Giant switchable Rashba effect in oxide heterostructures. *Adv Mater Interfaces* 2015; **2**: 1400445.

26. Caviglia AD, Gabay M and Gariglio S *et al.* Tunable Rashba spin-orbit interaction at oxide interfaces. *Phys Rev Lett* 2010; **104**: 126803.

27. Lin W, Li L and Doğan F *et al.* Interface-based tuning of Rashba spin-orbit interaction in asymmetric oxide heterostructures with 3d electrons. *Nat Commun* 2019; **10**: 3052.

28. Eremeev SV, Nechaev IA and Koroteev YM *et al.* Ideal two-dimensional electron systems with a giant Rashba-type spin splitting in real materials: surfaces of bismuth tellurohalides. *Phys Rev Lett* 2012; **108**: 246802.

29. Sakano M, Bahramy MS and Katayama A *et al.* Strongly spin-orbit coupled two-dimensional electron gas emerging near the surface of polar semiconductors. *Phys Rev Lett* 2013; **110**: 107204.

30. Sante DD, Barone P and Bertacco R *et al.* Electric control of the giant Rashba effect in bulk GeTe. *Adv Mater* 2012; **25**: 509–13.

31. Meng YH, Bai W and Gao H *et al.* Ferroelectric control of Rashba spin orbit coupling at the GeTe(111)/InP(111) interface. *Nanoscale* 2017; **9**: 17957–62.

32. Hanakata PZ, Rodin AS and Park HS *et al.* Strain-induced gauge and Rashba fields in ferroelectric Rashba lead chalcogenide PbX monolayers (X=S, Se, Te). *Phys Rev B* 2018; **97**: 235312.

33. Cahangirov S, Topsakal M and Aktürk E *et al.* Two- and one-dimensional honeycomb structures of silicon and germanium. *Phys Rev Lett* 2009; **102**: 236804.

34. Xu Y, Yan B and Zhang HJ *et al.* Large-gap quantum spin Hall insulators in tin films. *Phys Rev Lett* 2013; **111**: 136804.

35. Murakami S. Quantum spin Hall effect and enhanced magnetic response by spin-orbit coupling. *Phys Rev Lett* 2006; **97**: 236805.

36. Wada M, Murakami S and Freimuth F *et al.* Localized edge states in two-dimensional topological insulators: ultrathin Bi films. *Phys Rev B* 2011; **83**: 121310.

37. Liu Z, Liu CX and Wu YS *et al.* Stable nontrivial Z_2 topology in ultrathin Bi (111) films: a first-principles study. *Phys Rev Lett* 2011; **107**: 136805.

38. Wang Y, Lv J and Zhu L *et al.* Crystal structure prediction via particle-swarm optimization. *Phys Rev B* 2010; **82**: 094116.

39. Wang H, Pi ST and Kim J *et al.* Possibility of realizing quantum spin Hall effect at room temperature in stanene/Al_2O_3(0001). *Phys Rev B* 2016; **94**: 035112.

40. Lu YH, Zhou D and Wang T *et al.* Topological properties of atomic lead film with honeycomb structure. *Sci Rep* 2016; **6**: 21723.

41. Koroteev YM, Bihlmayer G and Gayone JE *et al.* Strong spin-orbit splitting on Bi surfaces. *Phys Rev Lett* 2004; **93**: 046403.

42. Ozaki T. Variationally optimized atomic orbitals for large-scale electronic structures. *Phys Rev B* 2003; **67**: 155108.

43. Yu R, Qi XL and Bernevig A *et al.* Equivalent expression of $\mathbb{Z}_2$ topological invariant for band insulators using the non-Abelian Berry connection. *Phys Rev B* 2011; **84**: 075119.

44. Chen M, Peng JP and Zhang HM *et al.* Molecular beam epitaxy of bilayer Bi(111) films on topological insulator Bi_2Te_3: a scanning tunneling microscopy study. *Appl Phys Lett* 2012; **101**: 081603.

45. Su SH, Chuang PY and Chen SW *et al.* Selective hydrogen etching leads to 2D Bi(111) bilayers on Bi_2Se_3: large Rashba splitting in topological insulator heterostructure. *Chem Mater* 2017; **29**: 8992–9000.

46. Zhu H, Zhou W and Yarmoff JA. The growth of bismuth on Bi_2Se_3 and the stability of the first bilayer. *Thin Solid Films* 2018; **660**: 343–52.

47. Grazianetti C, De Rosa S and Martella C *et al.* Optical conductivity of two-dimensional silicon: evidence of dirac electrodynamics. *Nano Lett* 2018; **18**: 7124–32.

48. Chen MX, Zhong Z and Weinert M. Designing substrates for silicene and germanene: first-principles calculations. *Phys Rev B* 2016; **94**: 075409.

49. Kresse G and Furthmüller J. Efficient iterative schemes for ab initio total-energy calculations using a plane-wave basis set. *Phys Rev B* 1996; **54**: 11169–86.

50. Kresse G and Joubert D. From ultrasoft pseudopotentials to the projector augmented-wave method. *Phys Rev B* 1999; **59**: 1758–75.

51. Klimeš J, Bowler DR and Michaelides A. Chemical accuracy for the van der Waals density functional. *J Phys Condens Matter* 2009; **22**: 022201.